Cenozoic unroofing history of the Ladakh Batholith, western Himalaya, constrained by thermochronology and numerical modelling

Cite As: Kirstein, LA, Foeken, JPT, Van der Beek, P, Stuart, FM & Phillips, RJ 2009, 'Cenozoic unroofing history of the Ladakh Batholith, western Himalaya, constrained by thermochronology and numerical modelling' *Journal of the Geological Society*, vol 166, pp. 667-678.

Cenozoic unroofing history of the Ladakh Batholith, western Himalaya constrained by thermochronology and numerical modeling.

L.A. Kirstein[1]; J.P.T. Foeken[2]; P. van der Beek[3]; F.M. Stuart[2]; R.J.Phillips[1]

[1]School of GeoSciences, University of Edinburgh, West Mains Road, Edinburgh, EH9 JW, U.K.

[2]Isotope Geosciences Unit, SUERC, Rankine Avenue, Glasgow, G75 0QF, U.K.

[3]Laboratoire de Géodynamique des Chaînes Alpines, Université Joseph Fourier, BP 53, 38041 Grenoble, France.

Abstract

The Ladakh Batholith is part of the Transhimalayan Plutonic Belt that crops out north of the Indus suture zone. We propose that the exhumation history of the Ladakh Batholith is linked to the tectonic, magmatic and erosion history of the Karakoram terrane and south west Tibet. We present new multiple low temperature thermochronometry data (zircon (U-Th)/He, apatite fission track and apatite (U-Th)/He) to gain insight into the cooling history of the Ladakh Batholith and recognize key periods in the evolution of the region. From the Indus Valley northwards the ages decrease across the batholith for all three thermochronometers applied. A model is proposed in which magmatism in the Ladakh Batholith ceased in the Late Eocene and initial denudation was driven by topographic uplift due to collision. Southward tilting of the batholith occurred in the Late Palaeogene. This tilting resulted in an asymmetric topography with increasing elevation to the north. Strong erosion occurred in this northern region while the southern margin was affected by northwards thrusting of the Indus Molasse. For the first time, clear temporal and spatial variations in exhumation rate are identified in this region highlighting why sampling strategy is critical in documenting exhumation changes in active tectonic settings.

Long-term crustal scale tectonic and geomorphic processes have dramatic effects on the near-surface environment. Exhumation rates vary as a function of the rate of erosion or the rate of removal of overburden by tectonic processes and can be quantified using low temperature thermochronometry (e.g. (U-Th)/He dating). Here we focus on the Ladakh Batholith to constrain spatial and temporal changes in exhumation north of the Indus Suture Zone (ISZ) since collision of India with Eurasia in the Eocene.

In the India-Eurasia convergence zone the Ladakh Batholith occupies a geodynamically significant position. The 5 km high Tibetan Plateau lies to the east, Nanga Parbat and the western Himalayan syntaxis to the west, the Karakoram terrane to the north and the Indian plate to the south. The batholith is bordered by significant crustal scale structures including the Main Karakoram Thrust, the ISZ and the Karakoram Fault.

The Ladakh Batholith is part of the Transhimalayan Plutonic Belt; a Cretaceous-Palaeogene Andean- type magmatic arc that extends for ~2500 km (Fig. 1) from Afghanistan in the west to Bhutan in the east. This arc system lies 100-200 km north of the Himalaya and is now represented primarily by several major granite batholiths that run parallel to the strike of the mountain range (Fig. 1). The batholiths are located close to the southern margin of the Eurasian plate but north of the ISZ and are exposed at elevations > 3200 m above mean sea level. Their unroofing history potentially traces the response of the margin to continued India-Eurasia collision in the Cenozoic (e.g. Copeland *et al.*, 1995) and/or to changing internal plate stresses. In particular the deformation pattern around the Tibetan Plateau is thought to have changed in the Oligocene - Miocene with the development of crustal scale structures including the Karakoram Fault, and significant magmatism in the Karakoram terrane, which have both local and regional implications for exhumation (Dewey *et al.*, 1989; Harrison *et al.*, 1992; Fielding, 1996; Harris, 2007; Valli *et al.*, 2007). Crustal thickening and melting north of Ladakh is recorded in the formation of southern Karakoram intrusives, e.g. the Baltoro and Mango Gusar granites during the Oligocene-Miocene (Parrish & Tirrul, 1989; Searle & Tirrul, 1991).

The thermal evolution of the Ladakh Batholith is not well documented despite several dating studies (Choubey, 1987; Sorkhabi *et al.*, 1994; Clift *et al.*, 2002; Schlup *et al.*, 2003; Kirstein *et al.*, 2006). However it has been suggested from apatite fission

track dating that the region had cooled to below 120 °C (Sorkhabi *et al.*, 1994; Clift *et al.*, 2002; Kirstein *et al.*, 2006) and was actively eroding (Garzanti & van Haver, 1988; Sinclair & Jaffey, 2001; Clift et al., 2002) by the Early Miocene.

By combining multiple low temperature thermochronometers (zircon (U-Th)/He, apatite fission track and apatite (U-Th)/He) with numerical modeling we gain insight into the cooling history of the Ladakh Batholith and recognize key periods in the evolution of the region. This approach allows for the quantification of the thermal evolution of the batholith and the denudation history of the region during a period of major tectonic reorganization, magmatic intrusion and continued development of the Tibetan Plateau (e.g. Fielding, 1996; Williams *et al.*, 2001; Molnar, 2005).

Geological Setting

The calc-alkaline Andean-type Ladakh Batholith intrudes the Kohistan-Ladakh island arc terrane, which was sandwiched between Eurasia (the Karakoram terrane) and India during collision in the Early Cenozoic (Fig. 1b). The Ladakh Batholith is composed of multiple intrusions, with U-Pb crystallization ages ranging from 103 to 50 Ma (Honegger *et al.*, 1982; Weinberg & Dunlap, 2000).

The Ladakh Batholith is bound to the south by the ISZ, which generally separates the batholith from the deformed sedimentary successions of the Indus Molasse except where the molasse onlaps the batholith (Frank et al., 1977). The Indus Molasse comprises Eocene to Miocene sediments including siltstones, limestones and conglomerates (Searle *et al.*, 1990). The batholith forms the southern boundary of the Shyok tectonic belt, which is composed of Paleozoic to Eocene metasedimentary, volcanic and metamorphic rocks bound by WNW-trending thrusts (Srimal *et al.*, 1987) (Fig. 1b). The calc-alkaline andesites of the Khardung Formation (Fig. 2) are the extrusive equivalent of the Ladakh Batholith and dip 60° north-northwestward (Clift et al., 2002). The Tirit Batholith lies north of the Ladakh Batholith and crops out within the Shyok Suture Zone (SSZ) (Fig. 2). It has a U-Pb crystallisation age of 68 ± 1 Ma (Weinberg *et al.*, 2000), suggesting that it is part of the same magmatic event that produced the Ladakh Batholith. Several major structures bound the batholith to the north including the Karakoram Fault and the Main Karakoram Thrust (MKT) (Fig. 1b).

The Khalsar Thrust is interpreted to be the eastern extension of the MKT in Ladakh (Srimal *et al.*, 1987) (Fig. 2). In the Baltistan region of Pakistan, the MKT runs N60°W along the Shyok Valley and has thrust the Karakoram terrane onto the Ladakh

terrane in the late Miocene (Allen & Chamberlain, 1991). The MKT has also been traced as the reactivation of the Shyok suture along a steep- to vertical- brittle fault west of Ladakh (Pêcher & LeFort, 1999). The eastward continuation is, however, not well documented. Between the Ladakh and Tirit batholiths, in the Shyok Valley volcanic and sedimentary rocks are locally deformed with penetrative foliations and steep lineations developed (Weinberg & Dunlap, 2000). Shearing of granitoids and basalts is evident in the region around the Hund and Khar villages (Fig. 2). Much of the deformation is brittle and is associated with greenschist facies metamorphism (Weinberg *et al.*, 2000). Part of the Ladakh Batholith is undeformed but there is a diffuse deformation zone north of Leh and a penetrative ductile shear fabric is developed within the Thanglasgo shear zone (TSZ) (Fig. 2) which is thought to be Miocene in age (Weinberg & Dunlap, 2000; Jain *et al.*, 2003). Mylonitized gneiss is evident along the Leh-Khardung La route along with discrete shear zones with sub-horizontal and listric thrusts showing SW vergence (Jain *et al.*, 2003, this study).

The Karakoram Fault is a large scale (>750 km), right lateral strike-slip fault that dissects the eastern part of the Karakoram Batholith and juxtaposes Late Cretaceous-Palaeogene rocks of the Ladakh and Saltoro Ranges against Jurassic to Miocene rocks of the Karakoram terrane with an offset of between 40 and 150 km (Weinberg & Dunlap, 2000; Phillips *et al.*, 2004). The age of initiation, timing and magnitude of strike-slip motion on the Karakoram Fault remains controversial. Fault movement associated with pure strike slip, transpressional and transtensional regimes has been reported and estimates of the timing of initiation vary from >26 to <15 Ma (Searle, 1996; Lacassin *et al.*, 2004; Phillips *et al.*, 2004; Valli *et al.*, 2007).

Previous dating studies

Previous thermochronology studies (Ar-Ar and fission track dating) in the Ladakh Batholith were aimed at understanding the cooling and denudation history of the batholith (Choubey, 1987; Sorkhabi *et al.*, 1994; Clift *et al.*, 2002; Schlup *et al.*, 2003; Kirstein *et al.*, 2006). Biotite and hornblende Ar-Ar cooling ages range from 44 to 52 Ma (Clift *et al.*, 2002). Zircon fission track (ZFT) data are limited and ages from the Kargil and Kiari areas (Fig. 1) indicate Eocene cooling (Sorkhabi *et al.*, 1994; Kumar *et al.*, 2007). ZFT ages from the Khardung and Lyoma regions (Fig. 3), are Late Oligocene (~26 Ma and ~32 Ma respectively; Kirstein *et al.*, 2006; Kumar *et al.*, 2007). Apatite fission track (AFT) ages are more spatially extensive covering the region from

Kargil to Lyoma (Fig. 1, 3). AFT ages range from 4.8 to 44.1 Ma (Choubey, 1987; Sorkhabi *et al.*, 1994; Clift *et al.*, 2002; Schlup *et al.*, 2003; Kumar *et al.*, 2007) (Fig. 3). Pliocene AFT ages from near Chumatang, along the southern border of the batholith, are thought to be related to brittle faulting and hydrothermal fluids resetting the ages (Choubey, 1987). Yet, there remains an overall spread in AFT ages from 10 to 44 Ma (Fig. 3) (Sorkhabi *et al.*, 1994; Clift *et al.*, 2002; Kirstein *et al.*, 2006; Kumar *et al.*, 2007). This may represent slow cooling of the batholith from the Late Eocene to Miocene. A steep elevation profile from the Khardung-La region, spanning 1.3 km in elevation, was reported by Kirstein *et al.* (2006). On the basis of invariant age-elevation relationships for ZHe and AFT ages as well as long track lengths, a period of rapid exhumation of the batholith at ~22 Ma was proposed (Kirstein *et al.*, 2006). A similar section sampled by Kumar *et al.* (2007) suggests a lower rate of exhumation (0.1 km/Myr). However, no track length data were reported by these authors and there is considerable scatter in the data below 4700 m.

The wide geographical distribution of previous sampling efforts (Fig. 3) and the absence of fission-track length data hamper understanding of the detailed history of exhumation in the region. Furthermore, no attempt has previously been made to model the denudation of the batholith.

Sampling strategy

Fourteen samples of granite or granodiorite were collected from across the Ladakh region (Figs. 2, 4) (Appendix 1 http://www.geolsoc.org.uk/SUPXXXX). These data are complemented by a further six samples from a section between Leh and Khardung for which AFT and zircon and apatite (U-Th)/He ages have been reported by Kirstein *et al.* (2006) (Fig. 2, 4). Of these combined samples nineteen are from the Ladakh Batholith and one from the Tirit Batholith (TIRI 3240) north-west of Satti (Fig. 2). A north-south section was sampled across the batholith from Leh to Tirit with additional samples from along the southern and northern margins of the batholith (Fig. 4).

Methods

In order to document the low temperature thermal history of the Ladakh Batholith, we have applied zircon (U-Th)/He (~200°C), apatite fission track (120°C) and apatite (U-Th)/He (55°C) thermochronology. Apatite (12 samples) and zircon (10 samples) were separated from the 100-150 μm grain size fractions. Apatite fission-track

thermochronology was performed by Donelick Analytical Inc., using the external detector method following established protocols (Donelick, 1993) (Appendix 2 http://www.geolsoc.org.uk/SUPXXXX). Dpar values (the diameter of etched spontaneous fission tracks measured parallel to the c-axis), which are representative of the kinetics of annealing and chemical composition (Burtner *et al.*, 1994; Carlson *et al.*, 1999), have a narrow range from 1.6 to 2.3 μm (Table 1) in these samples. This suggests that all apatites are F-rich, as confirmed by etch pits that are generally of uniform size (0.45 ± 0.05 μm). Track length measurements are reported for all samples; only confined track-in-track (TINT) fission tracks were measured.

Ten duplicate zircon samples were dated using the (U-Th)/He (ZHe) technique. For each sample, between 1 and 3 grains were packed into 99.9% pure platinum tubes; He extractions follow the procedures of Foeken *et al.* (2006). U and Th extraction and analysis follow the procedures of Dobson *et al.* (2005). Analytical uncertainty for the method is 3%, calculated based on blank corrections, U and Th spike reproducibility and measurement of standards (Fish Canyon Tuff). Corrections for alpha recoil were calculated using both a tetragonal prism geometry (where no terminations were measured), or a prism with pyramidal geometry (Hourigan *et al.*, 2005). The recoil-corrected uncertainty on the reported He age is assumed to be 8% reflecting variability in size, zonation and geometry. See Appendix 3 http://www.geolsoc.org.uk/SUPXXXX for grain sizes. Weighted mean ages and standard deviations (1σ) are plotted in Fig. 4 and used for the thermal modeling. If the duplicate analyses did not reproduce within 2σ of the weighted mean the age has been excluded from further discussion e.g. Bas1. Apatite (U-Th)/He (AHe) age determinations follow the procedure established by Balestrieri *et al.* (2005). Correction for helium recoil loss was made using the procedures of Farley *et al.* (1996) and Hourigan *et al.* (2005). Analytical uncertainty for each sample is 3–6%, with total uncertainty for each age following the recoil correction assumed to be 10%. Weighted mean AHe ages and standard deviations (1σ) were calculated and plotted in Fig.4 and used in thermal modeling.

Results

Zircon (U-Th)/He Dating

ZHe ages (±2σ) are reported in Table 2 and Fig. 2. Sample ages vary from Oligocene (33 Ma) to Middle Miocene (13 Ma). The ZHe ages are considerably younger than the Cretaceous-Palaeogene U-Pb crystallization ages of the batholith (> 50 Ma - Weinberg & Dunlap, 2000), and most likely reflect cooling due to unroofing of the batholith. A distinct geographic distribution of the ages is observed, with a systematic decrease in age with distance from the Indus River which delineates the southern terminus of the batholith (Table 2, Figs. 2, 4). ZHe ages from samples from along the southern margin are the oldest and yield Oligocene (25-33 Ma) ages (Fig. 2, 4). Younger Miocene ZHe ages (22-24 Ma) are recorded from the central part of the batholith (Fig. 2, 4). These ages are indistinguishable from the ZHe ages reported by Kirstein *et al.* (2006) for the Khardung-La profile. Two samples from the northern margin of the batholith are the youngest and yield Early to Mid Miocene (17-13 Ma) weighted mean ages (Fig. 2, 4).

Apatite Fission-Track Ages and Lengths

Central AFT ages (±2σ) range from Oligocene (35 Ma) to late Miocene (6 Ma) (Table 1, Fig. 2). Mean track lengths vary from 13.0 to 14.8 μm (Table 1) and have a unimodal distribution suggesting simple cooling histories.

As with the ZHe ages, the AFT ages also show an apparent geographic distribution; AFT ages decrease with distance north of the Indus Valley (Figs. 2, 4). AFT ages of samples from the southern batholith margin and in the Basgo Valley are Oligocene in age (35-30 Ma) (Fig. 4). Track lengths vary from 13.1 to 14.8 μm. Two of these samples (Karu and Bas 4001) fail the chi-squared test suggesting that there is potentially some compositional variation in the granite and/or slow cooling through the partial annealing zone. This grain age dispersion is statistically best accounted for by reporting central ages. The AFT ages overlap the ZHe ages in this region (Fig. 2), suggestive of a phase of rapid cooling through the ZHe partial retention zone (PRZ) and AFT partial annealing zone (PAZ) during Oligocene time.

In the central part of the batholith, samples have central AFT ages of 18.1 and 21.1 Ma (Table 1, Fig. 2). These are within uncertainty of, and have similar track lengths to, those reported for the Khardung-La profile by Kirstein *et al.* (2006) (Fig. 2). Samples from the Nang Valley, to the east of the main transect, also yield Early Miocene ages (21.1 and 19.8 Ma) with long (>14.4 μm) track lengths (Table 1, Fig. 4).

The AFT ages are within error of the reported ZHe ages, implying rapid cooling (Fig. 4) around this time.

AFT ages from the northern margin of the batholith, bounded by the Shyok Valley, are considerably younger (5.7-6.9 Ma) than ages recorded by samples from the central and southern regions (18-35 Ma) (Figs. 2, 4). The sample analyzed from the Tirit Batholith is also young (6.8 Ma). As a result of the young history of these northern samples, fewer track lengths (<56 tracks) were recorded; however, mean track lengths are relatively long (>13.6 μm; Table 1) suggesting simple cooling trajectories.

Apatite (U-Th)/He Dating

AHe ages are consistently younger than the AFT and ZHe ages (Fig. 2, 4, Table 3). AHe ages from the southern margin are all Early Miocene with weighted-mean ages ranging from 18.5 Ma (Taru3595) to 21.8 Ma (Leh3295). AHe ages for the central (Khardung-La) region are Mid Miocene (~ 12-14 Ma, Kirstein *et al.*, 2006) (Fig. 4). The geographical distribution of the AHe ages is consistent with the pattern observed from the ZHe and AFT data (Fig. 4).

Thermal histories

The cooling history of selected samples was modeled using the HeFTy (v.1.5.6) code, which generates both forward and inverse models for low temperature thermochronometric systems (Ketcham, 2005). Only samples with high track counts (>100 tracks) and chi-squared vales > 0.1 (Table 1) were modeled to constrain thermal histories. Hund3250 from the northern edge is an exception, as this sample has only 17 track-length measurements. We included it, however, in order to generate a representative thermal history for the northern margin of the batholith (Fig. 2). Forward modeling of synthetic grain age and track length data was performed initially, for comparison with the measured data. Constraints included the crystallization age of the batholith (> 50 Ma) and a surface temperature of 10 °C; Dpar was used as the kinetic variable for AFT models (c.f Ketcham, 2005). Having generated a thermal history, where available the additional ZHe and AHe ages were added and the time temperature history was inverse modeled in order to generate a set of thermal histories that were consistent with the measured data for each sample, as reflected by

the goodness-of-fit (GOF) parameter (Ketcham, 2005). The resulting t-T paths for selected samples are presented in Figure 5.

Modeling of the track-length and age data of Bas1 (southern margin) (TL = 14.0 μm; 112 tracks) indicates rapid (>10 °C/km) cooling (Fig. 5a) in the Oligocene (>30 Ma) followed by much slower cooling (<2 °C/Ma) from the Late Oligocene to Pliocene. Leh3295 also from the southern margin displays a different cooling history, with substantial cooling (>20 °C/Ma) in mid-Oligocene times (30 - 25 Ma) (Fig. 5b). These samples illustrate the variation in cooling histories both with distance along the Indus margin and across the batholith. Minimal erosion-related cooling has occurred along the southern margin since the Oligocene (Fig. 5a-b), suggesting slow erosional exhumation since this time.

Thermal modeling of sample KHARS 5245 (central batholith) from Kirstein *et al.* (2006) (21.9 Ma; TL = 14.0 μm; 110 tracks) provides a best fit solution consistent with rapid cooling from early to mid Miocene times (~25-12 Ma) at a rate of ~14°C/Ma and slower cooling since the Mid Miocene (Fig. 5c). This thermal history is typical of samples from the central part of the batholith (e.g. Khardung La, Kirstein *et al.*, 2006).

Sample Hund3250 is characteristic of samples from the northern margin and illustrates significant cooling in the Late Cenozoic (9 - 4 Ma) at a rate of ~30°C/Ma. There is an apparent trend in the timing of major cooling across the batholith with samples in the north experiencing more recent rapid cooling (Fig. 5d). This spatial pattern directly relies on the measured age distribution for each thermochronometer and implies that significantly more exhumation has occurred in the north than the south since the Miocene. To generate such asymmetry, we envisage that the batholith has been domed and/or tilted since its emplacement.

Model of batholith evolution

The differences in thermal histories across the batholith and the apparent decrease in age to the north could be linked to either accelerated erosion due to changing climate factors and/or to topographic change linked to regional tectonics and erosion.

The climate in the western Himalaya during the Oligocene-Miocene is not well documented. East Asia is considered to have experienced a humid warm climate from early to middle Miocene times (Clift, 2006). As a result, sediment flux from East and SE Asia increased during this interval (Clift, 2006). Increased sediment flux to the

Indus delta in the Early-Mid Miocene has also been detected (Clift & Gaedicke, 2002) and can be used to suggest similar humid warm climatic conditions in the western Himalaya (e.g. Clift, 2006). Thus, climate may be important in driving denudation in this region, particularly in the Early Miocene prior to the development of a Himalayan rain shadow.

We have modeled the measured multi-thermochronometric data using a modified version of the finite element code 'Pecube' (Braun, 2003) with the aim of demonstrating quantitatively that doming (model DOME) and/or southward tilting (to generate increased relief in the north; model TOPO) of the batholith combined with erosion can generate the measured age variations. The aim is to reproduce the general northward younging of ages, to quantify the difference in exhumation and to further the discussion as to whether the thermal structure might be affected by known local erosional and sedimentological processes, or regional magmatic and tectonic processes.

3-D Numerical modeling

'Pecube' (Braun, 2003) is a 3D thermal-kinematic model allowing for the prediction of thermochronometric age patterns for any imposed exhumation and topographic history. The local exhumation history at any point *i* in the model is the sum of two components: a spatially constant "regional" exhumation rate, which is allowed to vary through time, and topographic growth or decline modeled as follows:

$$z_{i_{ini}} = z_{ini} - \beta\,(z_{ini} - z_i)$$

where z_i is the present-day elevation of point *i*, $z_{i_{ini}}$ is it's initial elevation, and the model parameters β and z_{ini} are the "topographic amplification factor" and the initial mean elevation respectively. Thus, the initial topography of the model can vary from a flat surface at elevation z_{ini} (for $\beta = 0$) to the same as the present-day topography ($\beta = 1$). We adapted the original model to allow z_{ini} to vary spatially, in order to model a tilting scenario. For points where topographic growth occurs ($z_i > z_{i_{ini}}$), local exhumation is correspondingly smaller than the regional exhumation, whereas for locations where elevation decreases through time ($z_i < z_{i_{ini}}$) the local exhumation is larger.

The model responds to the varying topographic load by flexural isostasy. Flexural as well as thermal parameters were kept fixed for all model runs (cf. Table 4). The present-day topography was extracted from USGS GTOPO30 1 km DEM data. The model was run for 32 Myr (i.e. from Mid-Oligocene times to present-day) and includes two distinct phases, the first one occurring from 32 to 20 Ma and a second phase from 20 Ma to the present.

Model DOME

In model DOME, z_{ini} = 1000 m and β = 0.05, such that the initial relief is extremely small (<70 m). During the 1st phase of the model run, this plateau is exhumed at a rate of 0.1 km/Myr, without topographic change. The modern topography is generated during the second phase, while regional exhumation rates increase to 0.25 km/Myr (from which local topographic growth should be subtracted).

The ages generated by model DOME reproduce well the AFT ages from the central portion of the batholith (Fig. 6a). The model also predicts the ZHe ages measured from the southern part of the batholith. However, because of the symmetric topographic growth of the batholith, it fails to account for the apparent age decrease toward the north and the older AFT and AHe ages along the southern margin. Increasing the imposed regional exhumation rates to 1km/Myr and 0.5 km/Myr during the first and second phase of the model respectively, as suggested by thermal modeling using the HeFTy program, results in similar ZHe ages along the southern and northern margins (~25 Ma) and fails to reproduce the measured northward younging.

Model TOPO

Thermal modeling of the age (ZHe, AFT and AHe) and track-length data using the HeFTy program provides evidence of rapid cooling across the batholith at different time intervals. In our best-fit model TOPO we combine high exhumation rates (>0.4 km/Myr) with strong relief change in the northern part of the batholith to generate best fit curves for the three sets of data (Fig. 6b).

In this model, z_{ini} varied spatially from 1500 m in the south to 7500 m in the north, in order to generate a tilted topography. As in model DOME, an initial phase of exhumation only, at a rate of 0.75 km/Myr, was followed by a second phase of relief

change combined with a regional exhumation rate of 0.4 km/Myr. These values are consistent with the apparent rates generated by the HeFTy thermal modeling assuming a high initial geothermal gradient (>40 °C/km). Note that using a spatially varying z_{ini} is just an efficient way to model tilting as the near-surface thermal structure (with respect to the surface) is similar for a horizontal and long-wavelength tilted surface.

This model predicts a younging of all thermochronometer ages to the north, which broadly overlap with the measured ages in the central and northern regions (Fig. 6b). The older ZHe ages along the southern margin are also predicted, although model ages are still younger than those measured (23-27 Ma versus 26-33 Ma, respectively). The modeled age range for the AFT and AHe chronometers are too young along the southern margin (Fig. 6b).

From these 3D models it is apparent that the unroofing of the Ladakh Batholith is a complex process and potentially reflects a mixture of southward tilting to provide asymmetric relief change and initial updoming of the surface to generate the observed age distribution. The models are consistent in predicting high exhumation rates (>0.4 km/Myr) and strengthen the proposal that significant relief change (~ 5-6 km) must have occurred in the north.

This strongly suggests an important regional control on the unroofing history of the batholith. The old ages on the southern Indus margin are only just reproduced by our best-fit TOPO model. In the following sections we discuss a potential mechanism for offsetting denudation of the southern margin by thrusting of the Indus Molasse northwards and blanketing the lower reaches of the Ladakh Batholith in this region (e.g. Jamieson *et al.*, 2004), and the general regional setting during the Mid Cenozoic.

Discussion

Sedimentary record

If the Ladakh Batholith has been eroding since the Oligocene, a record of the erosion history is potentially preserved in the Indus Molasse. The Indus Group sediments were accumulated in an intra-montane continental setting between the batholith and the Himalaya (Garzanti & van Haver, 1988). Within the upper part of the succession several conglomeratic units, including the Hemis conglomerate and the Choksi conglomerate, crop out (Sinclair & Jaffey, 2001). The Hemis conglomerate is in places greater than 1.5 km thick and almost entirely (>90%) composed of clasts derived from

the Ladakh Batholith (Garzanti & van Haver, 1988). Further west, towards Kargil, the proportion decreases to less than 5% of the total section (Searle *et al.*, 1990). There are limited age constraints on these conglomerate units. Garzanti & van Haver (1988) suggested that they are Late Eocene-Early Oligocene, while more recently, Sinclair & Jaffey (2001) proposed an Early Miocene age. Recently Wu et al. (2007) showed that the Choksi conglomerate was deposited later than 45-41 Ma. The new thermochronometric data presented here suggests that portions of the Ladakh Batholith were exhumed from the Oligocene to Miocene, thus potentially shedding vast quantities of material into the intra-montane basin.

The Indus Molasse has been thrust northwards towards the Ladakh Batholith during the Neogene. Miocene AFT ages (13-14 Ma) from within the molasse record the thermal resetting of the apatite as a result of this thrust activity (e.g. Clift *et al.*, 2002). Indus Molasse sediments onlap and overlie intrusives of the Ladakh Batholith (Frank et al., 1977; Garzanti & van Haver, 1988). Jamieson *et al.* (2004) investigated the morphometry of catchments draining the Ladakh Batholith and described significant north-south asymmetry in catchment characteristics, particularly in the region sampled during this study. Basins draining toward the SW into the Indus River are smaller, shorter and proportionally thinner, and have lower mean elevations than those that drain NE towards the Shyok River. Particular note is made of the extensive accumulation of alluvium and colluvium in the SW draining tributaries (Jamieson *et al.*, 2004). It is suggested that extensive accumulation of sediment occurred and blanketed the batholith as a result of thrusting of the Indus Molasse northwards for the past ~20 Ma (Sinclair & Jaffey, 2001; Jamieson *et al.*, 2004). Sediment blanketing of the lower reaches of the Ladakh Batholith could potentially armor the bedrock against erosion and result in the modeled erosional asymmetry. Without this blanketing effect the angle of tilt would be very steep. It is also notable that the Nang Valley has not been affected by this blanketing and the AFT ages are Miocene, similar to the central batholith samples, suggesting that such a blanketing effect may be localised.

Cooling of the Transhimalayan Plutonic Belt

Fission-track dating has been used to investigate the cooling histories of samples from other parts of the Transhimalayan Plutonic Belt (Copeland *et al.*, 1987, 1995; Harrison *et al.*, 1997). An episode of rapid Early Miocene cooling has been reported from a number of areas where vertical sampling strategies were employed, including at Mount

Kailas (Harrison *et al.*, 1997) and Xizang, Quxu, Pachu and Gu Rong in Tibet (Copeland *et al.*, 1987; 1995) (Fig. 1). This rapid cooling supports a model of crustal shortening along a south-directed thrust (the Gangdese thrust) coupled with erosion of steep topography (Copeland *et al.*, 1995), suggesting a hybrid relief-tectonic model whereby thrusting plays an important role in generating topography.

The area sampled during this study is more extensive and it is evident from the thermal models that significant cooling of the southern margin of the batholith adjacent to the Indus Valley occurred in the Oligocene, followed by slower cooling since the Early Miocene. This slow cooling is also consistent with fission track data reported from high elevations in the Tso Morari dome to the SE (Schlup *et al.*, 2003) suggesting contemporaneous regional slow and steady exhumation since at least early Miocene times.

The age-invariant nature of samples from the central part of the Ladakh Batholith and thermal modeling of these age and track length data provides evidence for rapid cooling of this region in the Early Miocene, which slowed from the Mid Miocene. A similar scenario is envisaged further east in Tibet (e.g. Copeland *et al.*, 1995). However, in the northern region bordering the Shyok Valley, rapid cooling occurred from the Middle Miocene to Early Pliocene (Fig. 5d). These data indicate significant regional and temporal variations in denudation patterns following the generation of significant topography by southward tilting and doming of the batholith.

Uplift and dissection of the southwest margin of the Tibetan Plateau

The Tibetan Plateau is composed of a number of approximately east-west trending terranes including the Songpan-Ganzi, Qiangtang and Lhasa blocks (Yin & Harrison, 2000). The Qiangtang and Lhasa blocks are currently separated from the Ladakh Batholith by the Karakoram Fault (Phillips *et al.*, 2004) (Fig. 1). Dissection of the southern margin of the Tibetan Plateau and ultimately the development of the major Karakoram strike slip fault may have played a significant role in the latter stage of exhumation of the Ladakh Batholith in the studied region by forming a crustal-scale zone of weakness that allowed the sutured arc terrane to act as an independent block. Mylonites and localized shearing along the Karakoram Fault are recorded since mid Miocene times (Phillips *et al*., 2004). The development of this regional structure and overall dissection of the southwestern Tibetan Plateau coincide with key periods in the cooling history of the Ladakh Batholith.

Oligocene-Miocene intrusive activity in the Karakoram Terrane

North of the Ladakh Batholith lies the Karakoram Terrane. Initial magmatic activity in the Karakoram Terrane was related to subduction as the Indian Plate drifted northwards. However the intrusion of the Mango Gusar, Masherbrum and Baltoro plutons (Fig. 1) in the Oligocene and Miocene post-date the end of subduction (e.g. Parrish & Tirrul, 1989; Searle & Tirrul, 1991). These plutons and associated dykes demonstrate that the Karakoram region was characterized by high heat flow since ~ 25 Ma. Geochemical arguments based on hafnium and neodymium isotope analyses led Mahéo *et al.* (2002) to suggest that the gneisses and granites were generated as a result of a vast thermal anomaly related to break-off of the Indian continental lithosphere below Asia in the late Oligocene. The response of the lithosphere north of the Indus Suture Zone to this thermal anomaly may have been important in generating the proposed topographic asymmetry. Irrespective of the mechanism that generated the magmatism it is apparent that north of Ladakh the lithosphere was hot and deforming with buoyant upwelling generating topographic relief.

Unroofing the Ladakh Batholith

From the new thermochronometry data and numerical modeling presented here, we propose that the unroofing of the batholith occurred in a number of stages that were regulated by the regional tectonic and magmatic framework.

Stage 1. 49-30 Ma.

If the timing of India-Eurasia collision is marked by the cessation of magmatism in the Transhimalayan Plutonic Belt, as proposed by Weinberg & Dunlap (2000), then collision in this region occurred in the Eocene (Fig. 7a). Collision resulted in initial northward tilting of the Khardung Formation volcanic rocks. The collision was associated with topographic uplift and doming. It has been proposed that cooling of the batholith to <150 °C occurred by the Late Oligocene (30 Ma) (Dunlap *et al.*, 1998; Clift *et al.*, 2002). ZHe and AFT age data from the southern part of the batholith close to the ISZ preserve the record of this cooling; however, further north the batholith remained hotter (>200°C) for longer, generating Miocene ZHe ages.

Stage 2. 30-15 Ma.

Southward tilting of the batholith occurred in the Oligocene - Miocene. This was contemporaneous with large scale changes in the regional tectonic and thermo-magmatic framework as uplift of the Tibetan Plateau occurred, magma was generated in the Karakoram terrane and major crustal faults were initiated, including the Karakoram Fault (Fig. 7b). Tilting of the batholith may be related to the same forces that generated the Neogene Karakoram granites (Fig. 7b). This tilting resulted in an asymmetric topography and increased exhumation (e.g. Model TOPO). ZHe and AFT ages from the central portion of the batholith overlap and much of the region cooled rapidly to below the AFT closure temperature (~120 °C) by the Early Miocene (~22 Ma). Northwards thrusting of the Indus Molasse was initiated pre ~20 Ma (Searle *et al.*, 1990) and we propose that this thrusting played a key role in mantling the surfaces of the southern margin with sediment in the region where Oligocene ages are measured (Fig. 7c).

Stage 3. 15-0 Ma

To the north, erosional denudation of the elevated topography accounts for the rapid cooling measured during this time period by the ZHe and AFT age and track length data. Slower exhumation and low rates of erosion have persisted since Pliocene times. The latter evolution may have been affected by overthrusting of the northern margin by the Karakoram Terrane along the MKT (Searle & Tirrul, 1991) (Fig. 7c).

Conclusions

The new multi-thermochronometric data presented here confirm that rapid cooling of part of the Ladakh Batholith occurred in early Miocene times and provide increasing support for large scale deformation and erosion of this part of the Transhimalayan Plutonic Belt during the mid Cenozoic. Similar geochonological and thermochronological evidence that supports rapid Miocene exhumation is available from southern Tibet (e.g. Quxu Pluton) (Copeland *et al.*, 1987), suggesting that a large-scale regional change in tectonic regime occurred at that time (e.g. Harrison *et al.*, 1992, Fielding 1996; Chung *et al.*, 2005). The development of major strike slip faults, such as the central segment of the Karakoram Fault that bounds the south western Tibetan margin and was initiated c. 15 Ma (Phillips *et al.*, 2004) was important in facilitating the changing pattern of exhumation in the Ladakh region.

We propose a model in which the Ladakh Batholith was tilted southwards during the emplacement of the Karakoram granites to the north in the late Oligocene, which resulted in a strong relief increase (~5-6 km) in the northern region of the batholith bordering the Shyok Valley. Strong erosion of this northern region occurred in mid Miocene times. Exhumation in the southern part of the batholith is limited by topographic growth, potentially due to overthrusting of the Indus Molasse in the Indus valley mantling the surface.

The thermochronometric record of Cenozoic unroofing of the Ladakh Batholith varies both spatially and temporally and is governed by the regional deformation and erosion history, which includes dissection of the SW part of the Tibetan Plateau, crustal melting and changing base levels influencing erosion, sedimentation and sediment flux.

Acknowledgements

We thank D. Chew and two anonymous reviewers for insightful and constructive comments. We are particularly grateful to H. Sinclair for field sampling and general discussions throughout the project and K. Dobson for laboratory assistance. This work was funded by a European Union Marie Curie fellowship HPMF-CT-2000-00515 to LAK.

References

ALLEN, T. & CHAMBERLAIN, C.P. 1991. Metamorphic evidence for an inverted crustal section, with constraints on the main Karakoram thrust, Baltistan, northern Pakistan. *Journal of Metamorphic Geology*, **9**, 403-418.

BALESTRIERI, M.L., STUART, F.M., PERSANO, C., ABBATE, E. & BIGAZZI, G. 2005. Geomorphic development of the escarpment of the Eritrean margin, southern Red Sea: Combined use of fission track and (U-Th)/He thermochronometry. *Earth and Planetary Science Letters*, **231**, 97-110.

BRAUN, J. 2003. Pecube: a new finite-element code to solve the 3D heat transport equation including the effects of a time-varying, finite amplitude surface topography. *Computers & Geosciences*, **29**, 787-794.

BURTNER, R.L., NIGRINI, A. & DONELICK, R.A. 1994. Thermochronology of Lower Cretaceous source rocks in the Idaho-Wyoming thrust belt. *American Association of Petroleum Geologists Bulletin*, 78, 1613-1636.

CARLSON, W.D., DONELICK, R.A. & KETCHAM, R. 1999. Variability of apatite fission track annealing kinetics I: Experimental results. *American Mineralogist*, **84**, 1213-1223.

CHOUBEY, V.M. 1987. Fission track geochronology of the southern part of the Ladakh batholith, Ladakh, northwest Himalaya. *Geoscience Journal*, **VIII**, 73-80.

CHUNG, S.-L., CHU, M.-F., ZHANG, Y. Q., XIE, Y. W., LO, C.-H., LEE, T.-Y., LAN, C.-Y., LI, X. H., ZHANG, Q., & WANG, Y. Z. 2005. Tibetan tectonic evolution inferred from spatial and temporal variations in post-collisional magmatism. *Earth Science Reviews*, **68**, 173–196.

CLIFT, P.D. 2006 Controls on the erosion of Cenozoic Asia and the flux of clastic sediment to the ocean. *Earth and Planetary Science Letters*, **241**, 571–590.

CLIFT, P.D., CARTER, A., KROL, M. & KIRBY, E. 2002. Constraints on India-Eurasia collision in the Arabian Sea region taken from the Indus Group, Ladakh Himalaya, India. *In*: CLIFT, P.D., KROON, D., GAEDICKE, C. & CRAIG, J. (eds) *The tectonic and climatic evolution of the Arabian Sea region*. Geological Society Special Publications, London, 97-116.

CLIFT, P. & GAEDICKE, C. 2002. Accelerated mass flux to the Arabian Sea during the middle to late Miocene. *Geology*, **30**, 207-210.

COPELAND, P., HARRISON, T.M., KIDD, W.S.F., XU, R.H. & ZHANG, Y.Q. 1987. Rapid Early Miocene acceleration of uplift in the Gangdese Belt, Xizang (Southern Tibet), and its bearing on accommodation mechanisms of the India-Asia collision. *Earth and Planetary Science Letters*, **86**, 240-252.

COPELAND, P., HARRISON, T.M., YUN, P., KIDD, W.S.F., RODEN, M. & YUQUAN, Z. 1995. Thermal evolution of the Gangdese batholith, southern Tibet: A history of episodic unroofing. *Tectonics*, **14**, 223-236.

DEWEY, J.F., CANDE, S. & PITMAN, W.C. 1989. Tectonic evolution of the India Eurasia collision zone. *Eclogae Geologicae Helvetiae*, **82**, 717-734.

DOBSON, K.J., OLIVE, V., PERSANO, C. & STUART, F.M. 2005. A new procedure for the routine zircon (U-Th)/He age measurement. *Geophysical Research Abstracts*, **7**, EGU05-A-06696.

DONELICK, R.A. 1993. A method of fission track etching utilizing bulk chemical etching of apatite, U.S. Patent Number 5,267,274.

DUNLAP, W. J., WEINBERG, R. F. & SEARLE, M. P. 1998. Karakoram fault zone rocks cool in two phases. *Journal of the Geological Society,* **155**, 903-912.

FARLEY, K.A., WOLF, R.A. & SILVER, L.T. 1996. The effects of long alpha-stopping distances on (U-Th)/He ages. *Geochimica et Cosmochimica Acta*, **60**, 4223-4229.

FIELDING, E.J. 1996. Tibet uplift and erosion. *Tectonophysics*, **260**, 55–84.

FOEKEN, J.P.T., STUART, F.M., DOBSON, K., PERSANO, C. & VILBERT, D. 2006. A diode laser system for heating minerals for (U-Th)/He chronometry. *Geology Geophysics Geochemistry*, **7**, Q04015 doi.10.1029/2005GC001190.

FRANK, W, GANSSER, A. & TROMMSDORFF, V. 1977. Geological observations in the Ladakh Area (Himalayas). *Mineral. Petrogr. Mitt*., **66**, 13-27.
GANSSER, A. 1980. The significance of the Himalayan suture zone. *Tectonophysics,* **62**, 37-52.

GARZANTI, E. & VAN HAVER, T. 1988. The Indus clastics: forearc basin sedimentation in the Ladakh Himalaya (India). *Sedimentary Geology*, **59**, 237-249.

HARRIS, N.B.W. 2007. Channel flow and the Himalayan–Tibetan orogen: a critical review. *Journal of the Geological Society, London*, **164**, 511–523.

HARRISON, T.M., COPELAND, P., KIDD, W.S.F. & YIN, A.N. 1992. Raising Tibet. *Science*, **255**, 1663-1670.

HARRISON, T.M., RYERSON, F.J., LE FORT, P., YIN, A., LOVERA, O.M. & CATLOS, E. J. 1997. A late Miocene-Pliocene origin for the central Himalayan inverted metamorphism. *Earth and Planetary Science Letters*, **146**, E1-E7.

HONEGGER, K., DIETRICH, V., FRANK, W., GANSSER, A., THONI, M. & TROMMSDORFF, V. 1982. Magmatism and metamorphism in the Ladakh Himalayas (the Indus-Tsangpo suture zone). *Earth and Planetary Science Letters*, **60**, 253-292.

HOURIGAN, J.K., REINERS, P.W. & BRANDON, M.T. 2005. U-Th zonation-dependent alpha-ejection in (U-Th)/He chronometry. *Geochimica et Cosmochimica Acta*, **69**, 3349-3365.

JAIN, A.K., SINGH, S., MANICKAVASAGAM, R.M., JOSHI, M. & VERMA, P.K. 2003. HIMPROBE Programme: Integrated studies on geology, petrology, geochronology and geophysics of the Trans-Himalaya and Karakoram. *Memoir of the Geological Society of India*, **53**, 1-56.

JAMIESON, S.S.R., SINCLAIR, H.D., KIRSTEIN, L.A. & PURVES, R.S. 2004. Tectonic forcing of longitudinal valleys in the Himalaya: morphological analysis of the Ladakh batholith, N. India. *Geomorphology*, **58**, 49-65.

KETCHAM, R.A. 2005. Forward and inverse modeling of low temperature thermochronometry data. *In*: REINERS, P.W. & EHLERS, T.A. (eds.) *Low-temperature thermochronology: Techniques, Interpretations, and Applications*, The Mineralogical Society of America. *Reviews in Mineralogy and Geochemistry*, **58**, 275-314.

KIRSTEIN, LA., SINCLAIR, H., STUART, FM. & DOBSON, K. 2006. Rapid Early Miocene exhumation of the Ladakh batholith, western Himalaya. *Geology*, **34**, 1049-1052.

KUMAR, R., LAL, N.,SINGH, S. & JAIN, A.K. 2007. Cooling and exhumation of the Transhimalayan Ladakh batholith as constrained by fission track apatite and zircon ages. *Current Science*, **92**, 490-496.

LACASSIN, R., VALLI, F., ARNAUD, N., LELOUP, P.H., PAQUETTE, J.L., HAIBING, L., TAPPONNIER, P., CHEVALIER, M.-L., GUILLOT, S., MAHÉO, G. & ZHIQIN, X. 2004. Large-scale geometry, offset and kinematic evolution of the Karakorum fault, Tibet. *Earth and Planetary Science Letters*, **219**, 255-269.

MAHÉO, G., GUILLOT, S., BLICHERT-TOFT, J., ROLLAND, Y. & PÊCHER, A. 2002. A slab breakoff model for the Neogene thermal evolution of South Karakorum and South Tibet. *Earth and Planetary Science Letters*, **195**, 45-58.

MOLNAR, P. 2005. Mio-Pliocene Growth of the Tibetan Plateau and Evolution of East Asian Climate, Palaeontologia Electronica, **8**, 2-23.

PARRISH, R.P. & TIRRUL, R. 1989. U-Pb ages of the Baltoro granite, northwest Himalaya, and implications for monazite U-Pb systematics. *Geology,* **17**, 1076-1079.

PÊCHER, A. & LE FORT, P. 1999. Late Miocene tectonic evolution of the Karakorum-Nanga Parbat contact zone (northern Pakistan). *In:* MACFARLANE, A., SORKHABI, R.B. & QUADE, J. (eds.) Himalaya and Tibet: mountain roots to mountain tops. Boulder, Colorado, Geological Society of America Special Paper, 145-157.

PHILLIPS, R.J., PARRISH, R.P. & SEARLE, M.P. 2004. Age constraints on ductile deformation and long-term slip rates along the Karakoram Fault zone, Ladakh. *Earth and Planetary Science Letters*, **226**, 305-319.

SCHLUP, M., CARTER, A., COSCA, M. & STECK, A. 2003. Exhumation history of eastern Ladakh revealed by ^{40}Ar-^{39}Ar and fission track ages: the Indus River-Tso Morari transect, NW Himalaya. *Journal of the Geological Society*, *London*, **160**, 385-399.

SEARLE, M.P. 1996. Geological evidence against large-scale pre-Holocene offsets along the Karakoram Fault: implications for the limited extrusion of the Tibetan Plateau. *Tectonics*, **15**, 171-186.

SEARLE, M.P., PICKERING, K.T. & COOPER, D.J.W. 1990. Restoration and evolution of the intermontane Indus molasse basin, Ladakh Himalaya, India. *Tectonophysics*, **174**, 301-314.

SEARLE, M. P. & TIRRUL, R. 1991. Structural and thermal evolution of the Karakoram crust. *Journal of the Geological Society*, **148**, 65-82.

SINCLAIR, H.D. & JAFFEY, N. 2001. Sedimentology of the Indus group, Ladakh, northern India: implications for the timing of initiation of the palaeo-Indus River. *Journal of the Geological Society, London*, **158**, 151-162.

SORKHABI, R.B., JAIN, A.K., NISHIMURA, S., ITAYA, T., LAL, N., MANICKAVASAGAM, R.M. & TAGAMI, T. 1994. New age constraints on the cooling and unroofing history of the Transhimalayan Ladakh Batholith (Kargil area), N.W. India. *Proceedings of the Indian Academy of Science*, **103**, 83-97.

SRIMAL, N., BASU, A.R. & KYSER, T. K. 1987. Tectonic inferences from oxygen isotopes in volcano-plutonic complexes of the India-Asia collision zone, NW India. *Tectonics*, **6**, 261-273.

VALLI, F., ARNAUD, N., LELOUP, P.H., SOBEL, E.R., MAHÉO, G., LACASSIN, R., GUILLOT, S., LI, H., TAPPONNIER, P. & XU, Z. 2007. Twenty million years of continuous deformation along the Karakorum fault, western Tibet: A thermochronological analysis. *Tectonics*, **26**, TC4004.

WEINBERG, R.F., DUNLAP, W.J. & WHITEHOUSE, M. 2000. New field, structural and geochronological data from the Shyok and Nubra valleys, northern Ladakh; linking Kohistan to Tibet. *In:* KHAN, M.A., TRELOAR, P.J., SEARLE, M.P. & JAN, M.Q. (eds.) Tectonics of the Nanga Parbat syntaxis and the western Himalaya. *Geological Society of London*, **170**, 253-275.

WEINBERG, R.F. & DUNLAP, W.J. 2000. Growth and deformation of the Ladakh batholith, northwest Himalayas: Implications for timing of continental collision and origin of calc-alklaine batholiths. The Journal of Geology, 108, 303-320.

WILLIAMS, H., TURNER, S., KELLEY, S., HARRIS, N. 2001. Age of composition of dikes in southern Tibet: new constraints on the timing of east–west extension and its relationship to postcollisional magmatism. *Geology Geophysics Geochemistry*, **29**, 339–342.

WU, F-Y., CLIFT, P. D., YANG, J.-H. 2007. Zircon Hf isotopic constraints on the sources of the Indus Molasse, Ladakh Himalaya, India, *Tectonics*, **26**, TC2014, doi:10.1029/2006TC002051.

YIN, A. & HARRISON, T M. 2000. Geologic evolution of the Himalayan-Tibetan orogen. *Annual Reviews of Earth and Planetary Sciences*, **28**, 211-280.

Figures

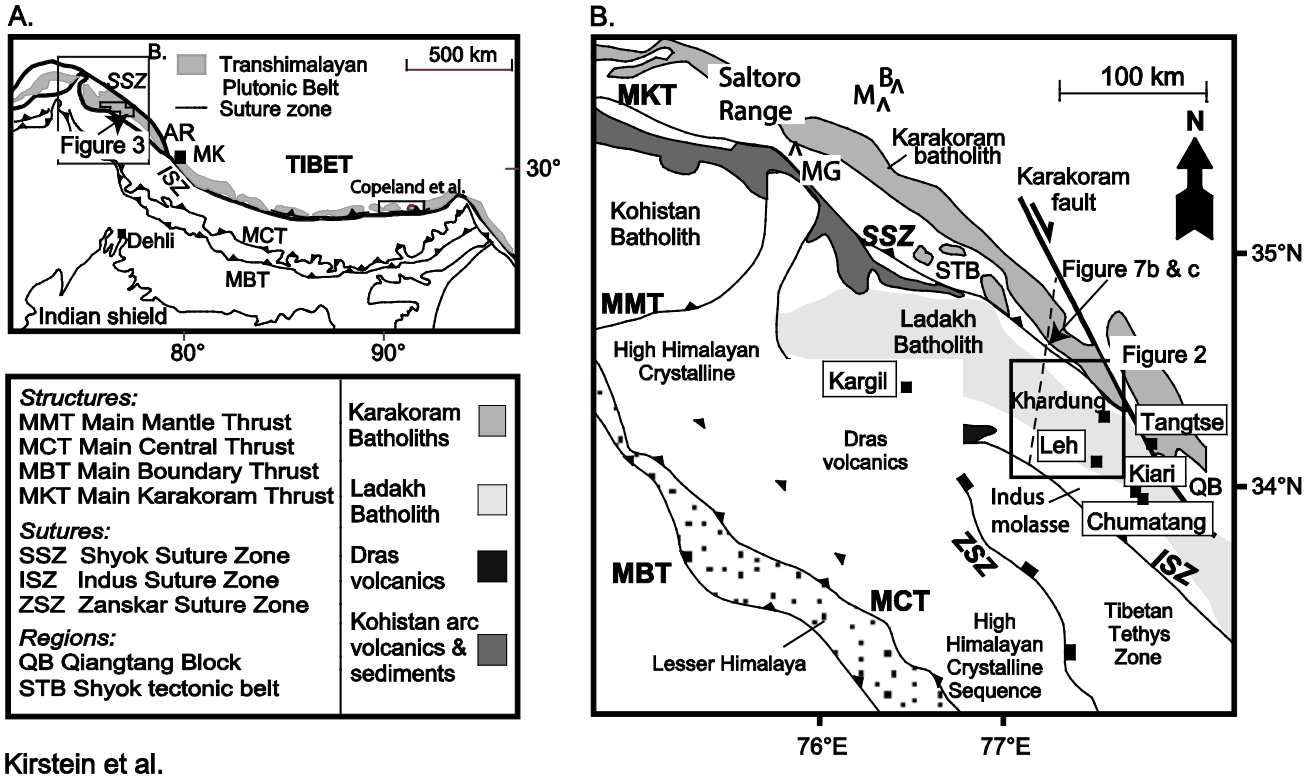

Kirstein et al.

Figure 1. A. Regional geological summary highlighting the Transhimalayan Plutonic Belt, the main suture zones and Himalayan structures. AR - Ayilari Range, location of Karakoram Fault segment dated by Valli *et al.* 2007. MK – Mount Kailas. Boxes indicate location of Copeland et al. (1995) study and figure 3. B. Detail of region of the Kohistan-Ladakh arc investigated including major regional structures and local place names referred to in the text. M – Masherbrum; B – Baltoro; MG – Mango Gusar. Dashed line indicates idealized line of section in Figure 7b & c.

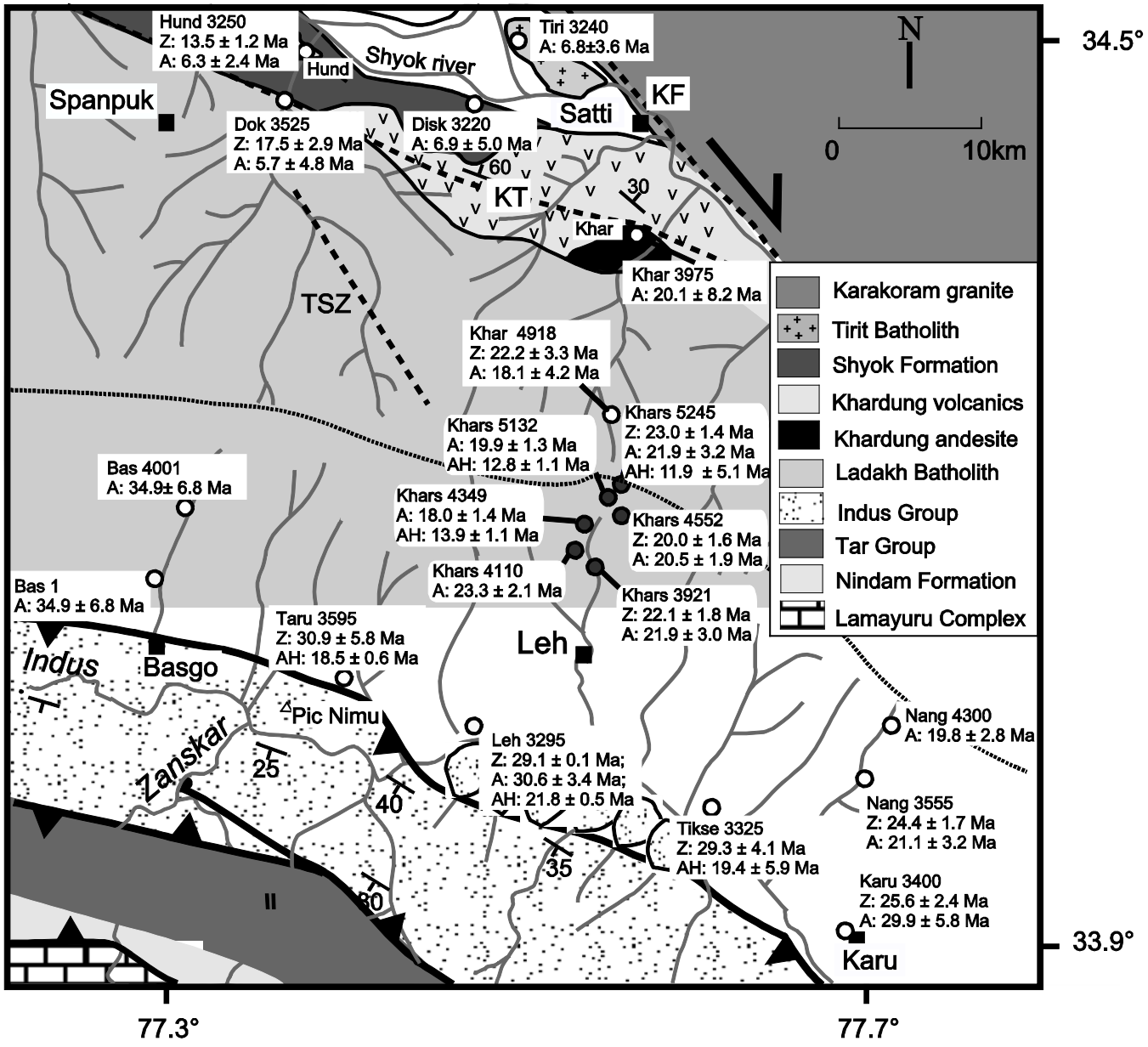

Figure 2. Geological map of the region of the Ladakh Batholith sampled during this study. Open circles indicate new sample sites along with new age data. Z = Zircon He age; A = Apatite fission track age; AH = Apatite He age. Quoted uncertainties are 2 sigma. Filled circles indicate sample sites previously reported by Kirstein *et al.*, 2006. Dashed lines indicate major structures including the Karakoram Fault (KF), the Thanglasgo shear zone (TSZ) and the Khalsar Thrust (KT). Dotted line indicates position of the main drainage divide.

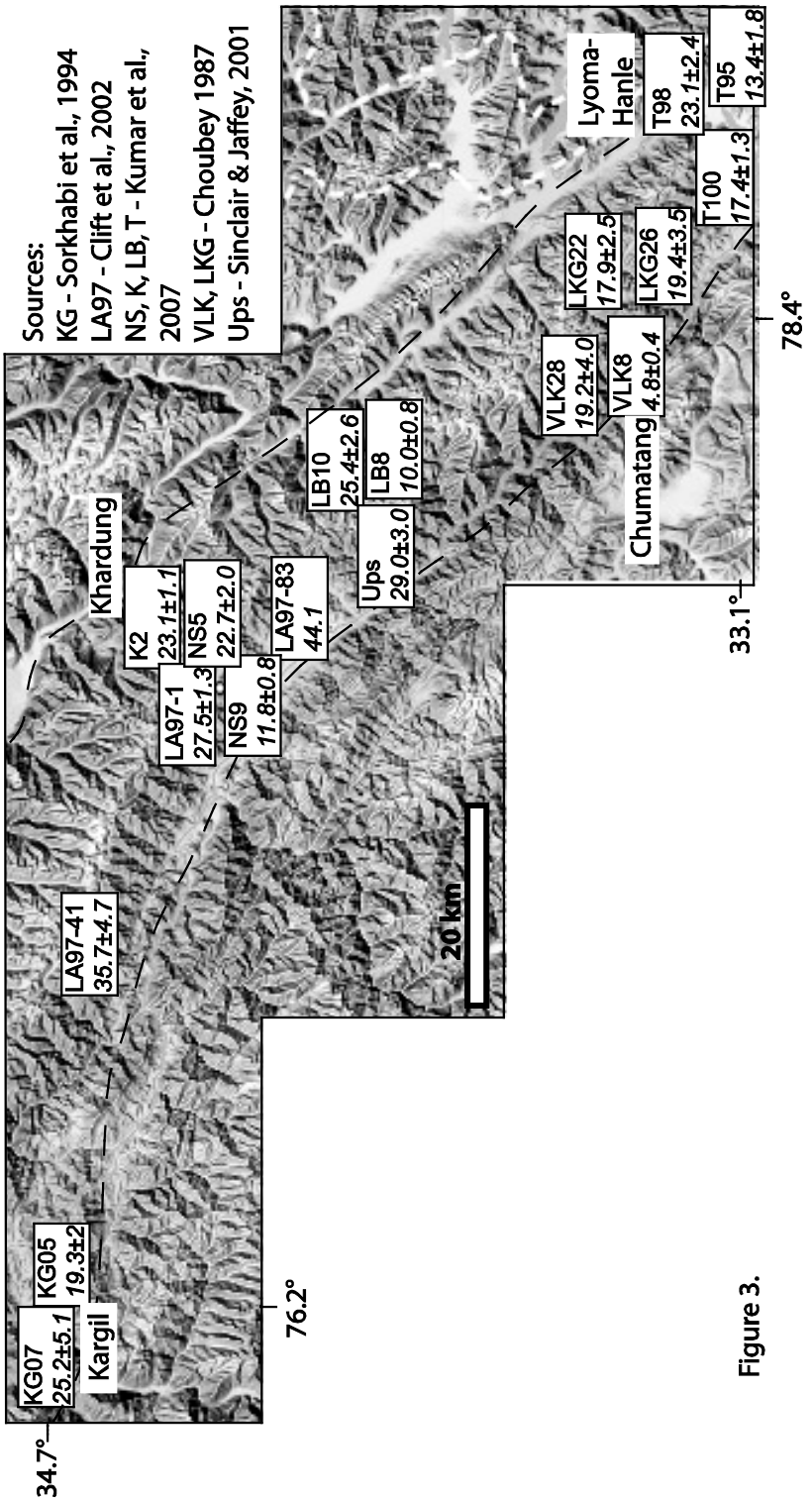

Figure 3.

Figure 3. Low resolution DEM of the Ladakh Batholith region highlighting the large areal distribution of samples previously dated by others including Choubey, 1987; Sorkhabi *et al.*, 1994; Sinclair & Jaffey, 2001; Clift *et al.*, 2002; Schlup *et al.*, 2003; Kumar *et al.*, 2007. Dashed lines indicate approximate edge of batholith.

Figure 4.

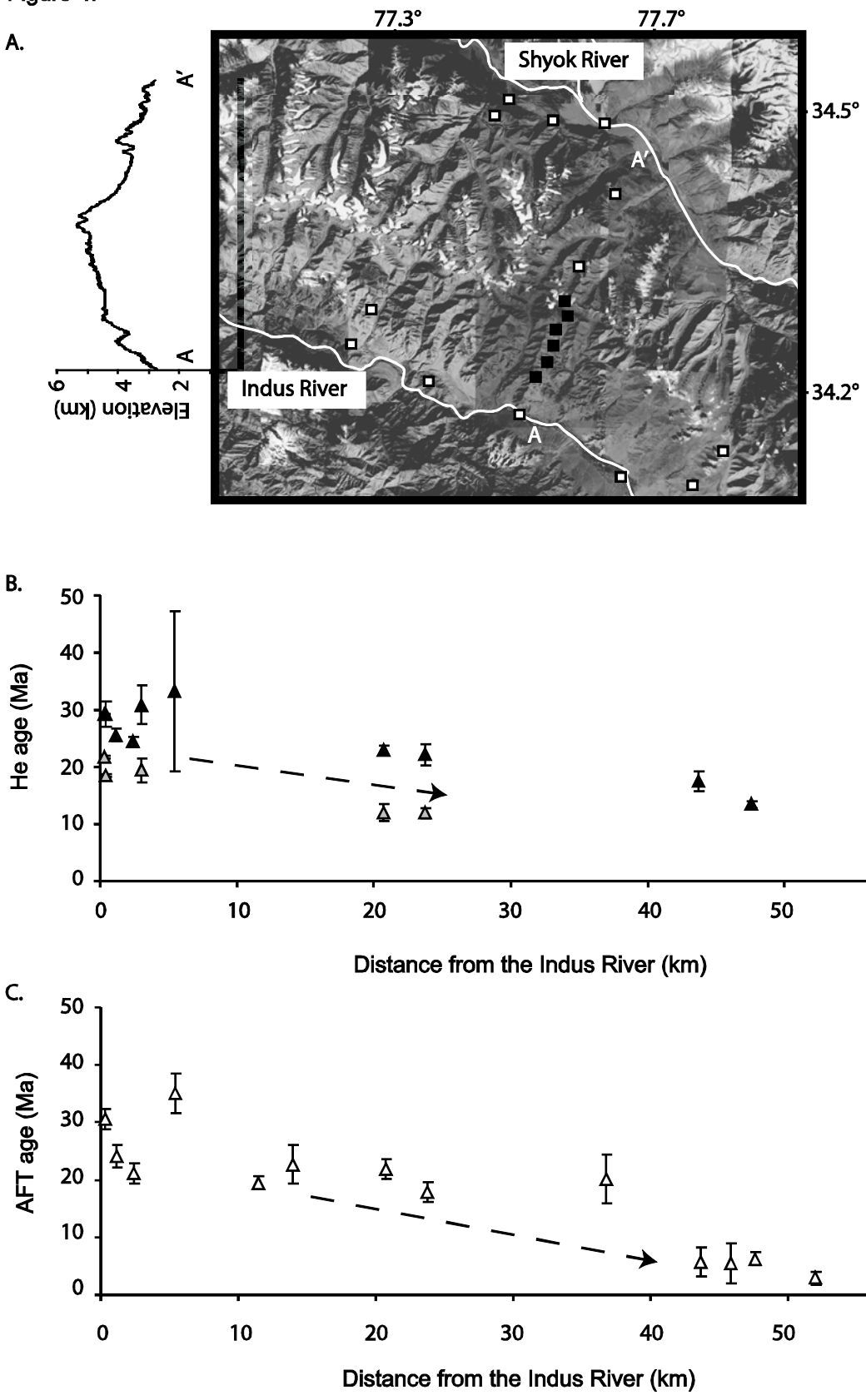

Kirstein et al.

Figure 4. A. Low resolution DEM of the Ladakh Batholith showing sample locations; white squares - new samples; black squares – data from Kirstein *et al.*, 2006. B. Zircon (black triangles) and apatite (grey triangles) He age data ± 1σ plotted against distance from the Indus River. C. Apatite fission-track (white triangles) age data ± 1σ plotted against distance from the Indus River. Note the systematic decrease of age from the south, near the Indus River, to the north towards the Shyok River, in both plots (indicated by dashed arrow).

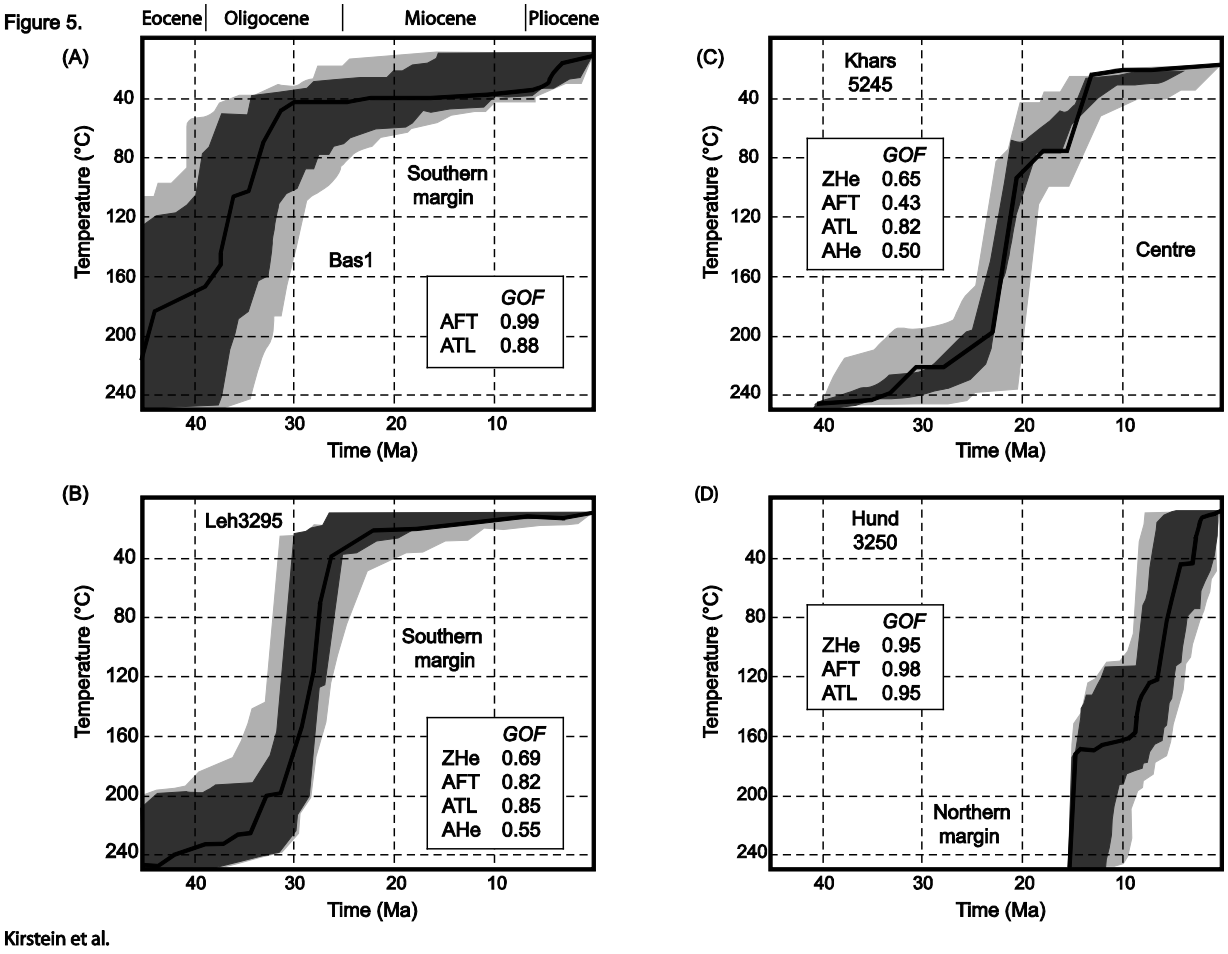

Figure 5. Selected thermal histories for samples from the south (A, B), the centre (C) and the north (D) of the batholith modeled using HeFTy (v.1.5.6) code (Ketcham, 2005). ATL = average track length. Note all samples indicate fast cooling from temperatures of ~200°C to ~80 °C although the timing of this cooling varies with location e.g. the south cooled at least 15 Myr before the north. GOF – goodness of fit criterion defined by Ketcham (2005). Dark grey area indicates good fit (GOF > 0.5); lighter grey acceptable fit (GOF >0.2) for thermal histories. ATL – apatite track length. Oligocene (38 – 25 Ma); Miocene (25 – 5.1 Ma); Pliocene (5.1-2.0 Ma).

Figure 6.

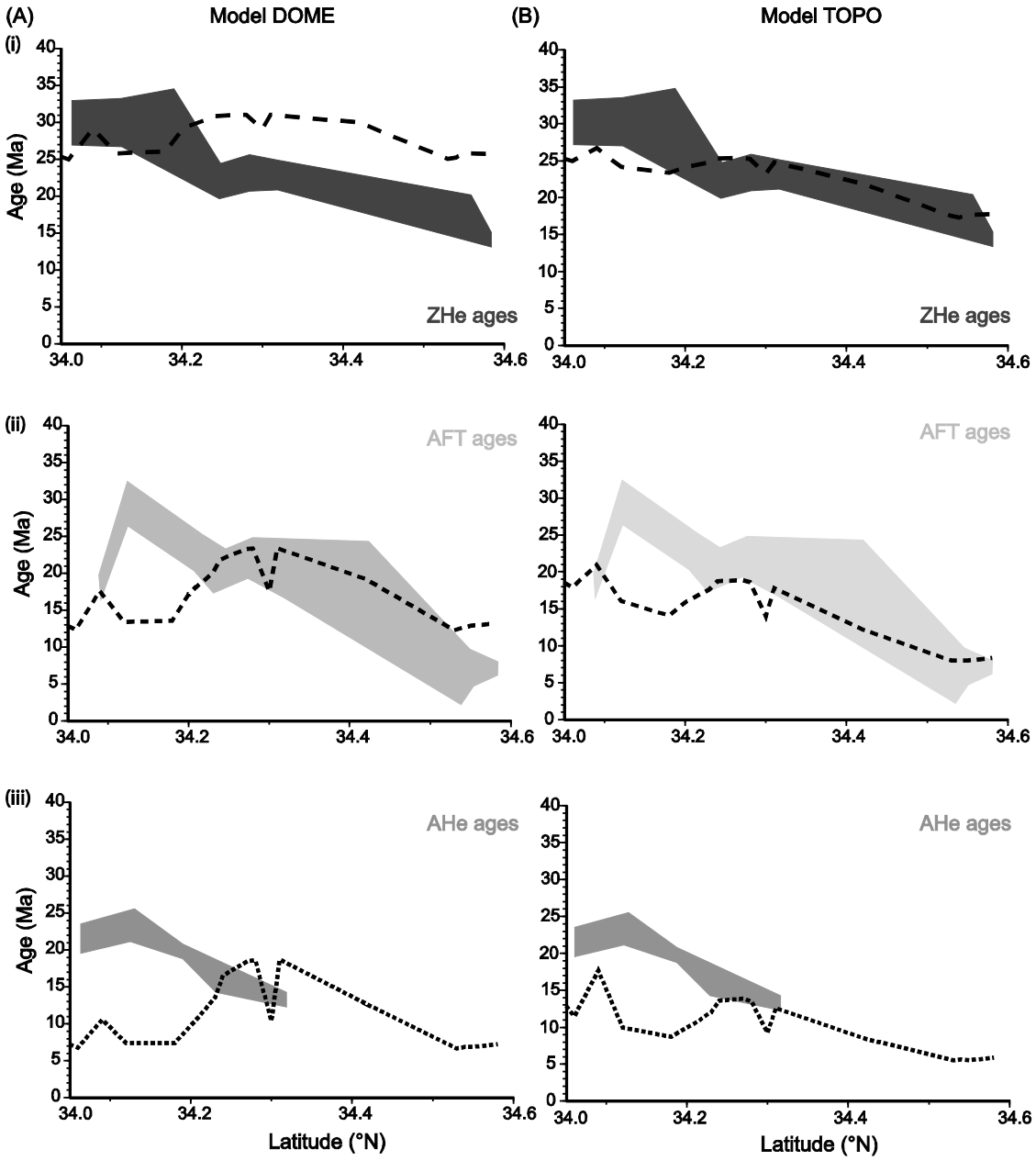

Figure 6. Comparison of results in the form of age versus latitude from best fit models (A) DOME and (B) TOPO generated using a modified version of the 'Pecube' finite element code (Braun, 2005) for each of the thermochrononmeters applied (i) ZHe; (ii) AFT; (iii) AHe. In model DOME exhumation rate changes from 0.1 km/Myr with no topographic change to 0.25 km/Myr with the generation of topography. In model TOPO exhumation rates varied from 0.75 km/Myr to 0.4 km/Myr. Dashed lines are best fit model results. Shaded regions correspond to measured data envelope for each thermochronometer. The age boundaries are formed by joining the upper error bars and the lower error bars. Note the limited AHe data (iii). Note also how well model TOPO fits the ZHe data (i) and reproduces the young AFT ages (ii) along the northern margin in comparison to model DOME.

Figure 7.

A. Stage 1 ~ 45 Ma.

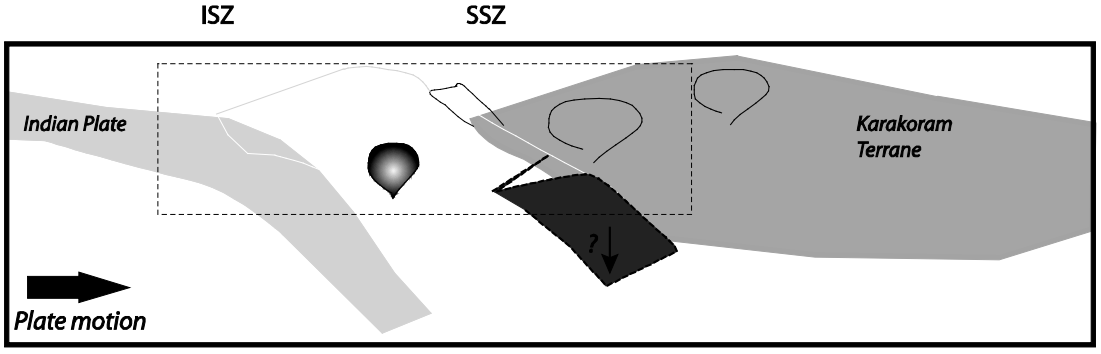

B. Stage 2 ~ 22 Ma.

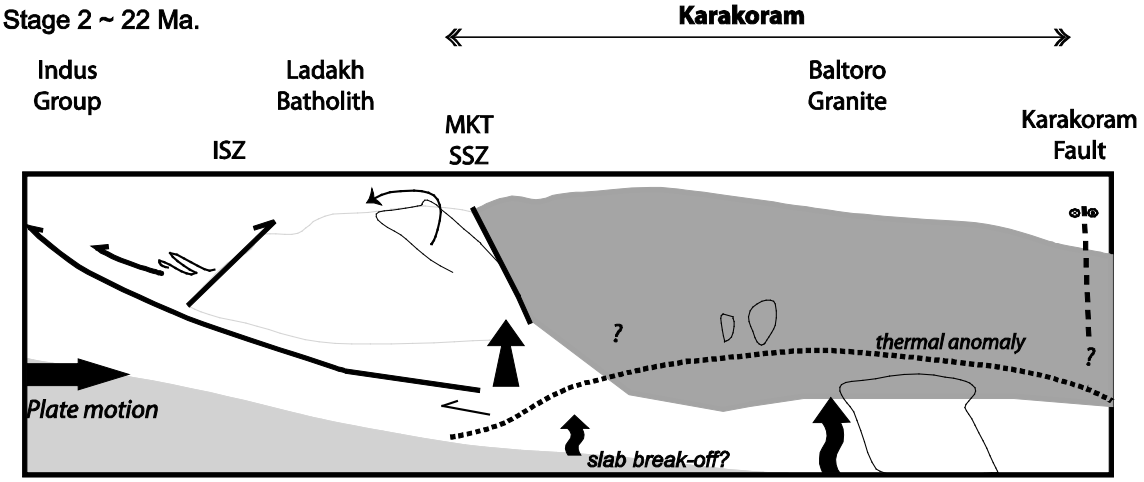

C. Stage 3 ~ 10 Ma.

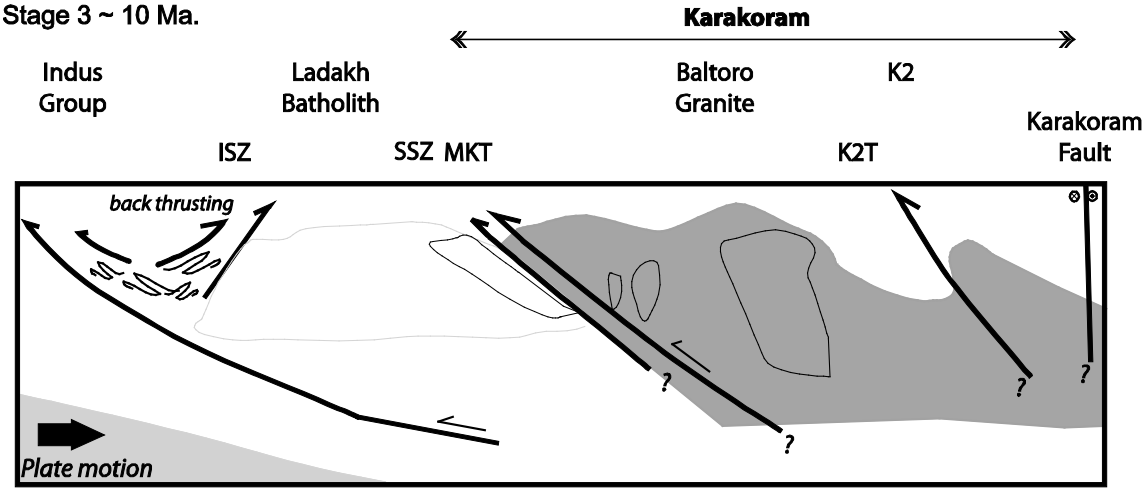

Kirstein et al.

Figure 7. Schematic cross-sectional model of the proposed evolution of the Ladakh Batholith from the timing of collision until the Late Miocene. During Stage 1 collision results in a cessation of magmatism, northwards tilting of the Khardung volcanic formation and doming of the batholith. Dashed rectangle is the focus of the discussion of stages 2 and 3 (parts B and C, respectively). B. Stage 2: the thermal anomaly associated with the generation of the Oligocene-Miocene Karakoram granites results in preferential uplift of the northern margin of the Ladakh Batholith resulting in an asymmetric topography. C. Stage 3: Backthrusting of the Indus Group mantles the southern margin of the batholith while to the north thrusting of the Karakoram terrane over the batholith occurs substantially changing the pattern of denudation. The structures including K2 thrust (K2T) based on those described by Searle & Tirrul (1991).

Table 1. Apatite fission track analyses for the Ladakh Batholith.

Sample	**Elevation** (m)	ρ_s (10^6 tracks cm^{-2})	N_s	ρ_I (10^6 tracks cm^{-2})	N_i	ρ_d (10^6 tracks cm^{-2})	N_d	**Grains**	**U** (ppm)	**Dpar** (μm)	**Central Age ± 2σ** (Ma)	**P(χ^2)**	**Tracks**	**Mean Length** (μm)	**SE** (μm)
Central batholith															
Khar 3975	3975	0.060	26	0.583	251	3.408	4215	25	10.1	1.78	20.1 ±8.2	0.583	23	13.0	0.56
Khar 4918*	4918	0.404	170	4.338	1824	3.389	4215	25	62.8	1.75	18.1 ±4.2	0.002	122	13.8	0.13
Nang 3555	3530	0.250	190	2.641	2010	3.929	4025	25	34.8	1.74	21.1±3.2	0.413	104	14.4	0.14
Nang 4300*	4300	0.424	384	4.432	4011	3.582	4215	25	60.6	2.10	19.8±2.8	0.016	132	14.6	0.13
Southern margin															
BAS1	3550	0.195	155	1.145	911	3.621	4215	25	14.2	1.70	34.9±6.8	0.348	112	14.0	0.12
BAS 4001*	4001	0.370	84	2.139	486	3.486	4215	21	31.0	2.18	33.8±9.6	0.060	113	13.7	0.18
LEH 3295	3295	0.895	462	5.565	2874	3.350	4215	24	75.1	2.29	30.6±3.4	0.278	137	14.8	0.12
Karu 3400*	3400	0.606	265	4.125	1803	3.447	4215	23	58.7	1.95	29.9±5.8	0.001	131	13.1	0.18
Northern margin															
Disk 3220	3220	0.020	8	0.581	229	3.466	4215	24	7.8	1.64	6.9 ±5.0	0.621	13	13.6	0.56
Dok 3525	3525	0.028	6	1.002	213	3.544	4215	25	13.4	1.59	5.7 ±4.8	0.586	4	14.5	0.98
Hund 3250	3250	0.077	28	2.506	906	3.563	4215	20	34.5	1.84	6.3 ±2.4	0.287	17	13.8	0.56
Tiri 3240*	3240	0.037	23	1.156	717	3.370	4215	25	15.7	1.81	6.8 ±3.6	0.012	56	14.1	0.25

Closure temperature ~120 °C (Carlson et al., 1999); * Samples with age dispersion >20%.

Table 2. Zircon (U-Th)/He age determinations for the Ladakh Batholith.

Sample		Elevation(m)	^{238}U (ng)	^{232}Th (ng)	^{4}He (cc)	No. crystals	He age (Ma)	Ft correction	Corrected He age (Ma) ± 1 σ	Weighted He age (Ma) ± 2 σ
Central Batholith										
Khars 5245	(i)	5245	4.600	2.275	1.08E-08	3	17.2	0.77	22.3±1.8	23.0±1.4
	(ii)		2.713	1.827	6.52E-09	2	17.0	0.72	23.7±1.9	
Khar 4918	(i)	4918	5.822	5.062	1.63E-08	2	19.1	0.79	24.1±1.9	22.2±3.3
	(ii)		5.653	5.410	1.38E-08	2	16.3	0.78	20.8±1.7	
Nang 3555	(i)	3555	4.742	4.637	1.17E-08	3	16.5	0.70	23.6±1.9	24.4±1.7
	(ii)		17.851	22.990	4.97E-08	3	17.6	0.70	25.3±2.0	
Southern margin										
BAS1	(i)	3550	1.930	2.065	1.02E-08	2	34.5	0.72	48.0±3.8	
	(ii)		6.314	4.496	1.76E-08	3	19.6	0.69	28.2±2.3	
LEH 3295	(i)	3295	2.592	1.842	8.18E-09	2	22.2	0.76	29.2±1.8	29.1±0.1
	(ii)		2.779	1.710	8.88E-09	3	22.9	0.79	29.0±2.3	
Karu 3400	(i)	3400	11.856	5.834	2.12E-08	2	20.0	0.74	26.9±2.2	25.6±2.4
	(ii)		9.042	3.765	1.63E-08	3	17.5	0.71	24.5±2.0	
Taru 3595	(i)	3595	2.701	2.158	9.91E-09	2	25.3	0.74	34.3±2.7	30.9±5.8
	(ii)		3.581	2.918	1.21E-08	2	23.2	0.81	28.5±2.3	
Tikse 3325	(i)	3325	9.108	5.219	2.91E-08	1	23.1	0.84	27.5±2.2	29.3±4.1
	(ii)		7.503	8.956	2.76E-08	2	23.5	0.74	31.6±2.5	
Northern margin										
Dok 3525	(i)	3525	7.673	8.963	1.78E-08	3	15.0	0.78	19.2±1.5	17.5±2.9
	(ii)		3.894	4.704	8.44E-09	1	13.9	0.85	16.3±1.3	
Hund 3250	(i)	3250	10.466	9.513	1.55E-08	3	10.0	0.78	12.9±1.0	13.5±1.2
	(ii)		12.537	9.449	1.95E-08	2	10.9	0.78	14.1±1.1	

Note: Closure temperature 200°C (Hourigan et al., 2005); Recoil corrections calculated assuming prism with pyramid terminations after Hourigan et al. (2005).

Table 3. Apatite U, Th and He data from the Ladakh Batholith.

Sample		Elevation (m)	^{238}U (ng)	^{232}Th (ng)	^{4}He (cc)	No. crystals	He age (Ma)	Ft correction	Corrected He age (Ma) ± 1σ	Weighted He age (Ma) ± 2σ
LEH3295	(i)	3295	0.839	1.620	2.70E-09	5	18.2	0.82	22.1±2.2	21.8±0.5
	(ii)		0.354	0.701	8.90E-10	4	14.1	0.65	21.6±2.2	
Tikse 3325	(i)	3325	0.009	0.028	3.29E-11	4	16.8	0.72	23.2±2.3	19.4±5.9
	(ii)		0.161	0.433	4.59E-10	5	17.3	0.83	17.3±1.7	
Taru 3595	(i)	3595	0.280	1.239	1.12E-09	6	16.0	0.88	18.2±1.8	18.5±0.6
	(ii)		0.478	1.974	1.85E-09	6	16.1	0.86	18.8±1.9	
Khar 4918	(i)	4918	0.192	0.589	3.32E-10	6	8.3	0.70	11.9±1.2	

Closure temperature AHe: 80-55°C (Farley, 2000). Total uncertainty for each age post recoil correction is 10%.

Table 4. Input parameters for Pecube 3D thermo-kinetic models

Parameter	Value
Flexural isostasy parameters	
Crustal density (kg/m^3)	2700
Mantle density (kg/m^3)	3200
Young's modulus (GPa)	100
Pascal ratio	0.25
Effective elastic thickness (m)	10^4
Thermal parameters	
Model thickness (m)	20x20x20
Thermal diffusivity (km^2/Myr)	25
Temperature at base of model (°C)	525
Temperature at sea-level (°C)	25
Atmospheric lapse rate (°C/km)	6

Supplementary data

Grain size dimensions zircon He anlayses

Sample	Khars 5245 (i)			Khars 5245 (ii)		Khar 4918 (i)		Khar 4918 (ii)
Grain	1	2	3	1	2	1	2	1
Length	128	76	78	154	152	196	96	220
Width 1	102	102	102	68	64	96	146	96
Width 2	105	79	79	68	64	96	122	72
# terminati	2	2	2	2	2	1	2	1
T1	51	51	51	25	30	44	72	73
T2	76	51	25	51	38	0	96	0

Sample	Nang 3555 (i)			Nang 3555 (ii)			
Grain	2	1	2	3	1	2	3
Length	144	134	144	98	167	140	142
Width 1	110	82	80	61	102	51	77
Width 2	96	51	75	51	79	51	51
# terminati	2	2	1	2	1	2	2
T1	48	30	24	25	38	25	25
T2	48	20	0	20	0	40	38

Sample	Bas 1(ii)			Bas 1(i)		Leh 3295 (i)		Leh 3295 (ii)
Grain	1	2	3	1	2	1	2	1
Length	129	108	155	115	172	125	60	120
Width 1	80	88	76	85	62	130	130	135
Width 2	76	80	40	72	60	125	110	100
# terminati	2	2	2	2	2	2	2	2
T1	22	31	25	24	30	30	60	40
T2	19	31	28	30	20	35	60	40

Sample	Leh 3295 (ii)		Karu 3400 (i)		Karu 3400 (ii)			Taru 3975 (i)
Grain	2	3	1	2	1	2	3	1
Length	85	75	182	146	91	70	139	172
Width 1	140	110	97	85	98	98	73	80
Width 2	90	85	82	63	92	85	59	60
# terminati	2	2	2	2	2	2	2	2
T1	50	40	36	30	38	30	23	36
T2	40	35	36	42	38	38	30	36

Sample	Taru 3975	Taru 3975 (ii)		Tikse 3325	Tikse 3325 (i)		Dok 3525 (i)	
Grain	2	1	2	1	1	2	1	2
Length	158	232	291	159	158	134	185	180
Width 1	80	97	109	182	96	96	100	140
Width 2	72	97	97	144	51	75	60	92
# terminati	2	2	1	2	2	1	2	1
T1	30	35	72	96	48	48	50	80
T2	30	35	0	60	48	0	25	0

Sample	Dok 3525 (	Dok 3525 (	Hund 3250 (i)			Hund 3250 (ii)	
Grain	3	1	1	2	3	1	2
Length	150	255	73	96	97	121	85
Width 1	100	160	97	96	96	115	97
Width 2	90	150	91	84	96	97	85
# terminati	2	1	2	0	2	2	2
T1	40	45	24	0	24	36	36
T2	30	0	24	0	24	24	48

Grain size dimensions apatite He anlayses

Sample	Leh 3295 (i)					Leh 3295 (ii)		
Grain	1	2	3	4	5	1	2	3
Length	178.2	130.2	124	111.6	99.2	136.4	148.8	136.4
Width	59.4	62	80.6	74.4	49.6	80.6	86.8	74.4
# terminati	1	1	0	1	1	0	1	1

Sample	Leh 3295 (	Tikse 3325 (i)				Tikse 3325 (ii)		
Grain	4	1	2	3	4	1	2	3
Length	99.2	173.6	148.8	186	161.2	186	235.6	136.4
Width	55.8	99.2	74.4	86.8	86.8	62	62	62
# terminati	1	1	1	0	1	1	0	0

Sample	Tikse 3325 (ii)		Taru 3595 (i)					
Grain	4	5	1	2	3	4	5	6
Length	86.8	148.8	632	395	553	474	116	194
Width	74.6	86.8	158	316	158	158	395	395
# terminati	1	1	2	1	1	2	0	1

Sample	Taru 3595 (ii)					
Grain	1	2	3	4	5	6
Length	434.5	316	316	553	316	474
Width	237	158	118.5	197.5	158	158
# terminati	0	1	0	1	1	1

Sample	Khar 4918					
Grain	1	2	3	4	5	6
Length	194	194	194	97	116	194
Width	78	78	78	78	78	78
# terminati	1	0	1	1	1	0